

# Evaluation of homogenized thermal conductivities of imperfect carbon-carbon textile composites using the Mori-Tanaka method

Jan Vorel<sup>a</sup> and Michal Šejnoha<sup>a,b</sup>,

<sup>a</sup>*Department of Mechanics, Faculty of Civil Engineering, Czech Technical University in Prague, Thákurova 7, 166 29 Prague 6, Czech Republic*

<sup>b</sup>*Centre for Integrated Design of Advances Structures, Thákurova 7, 166 29 Prague 6, Czech Republic*

---

## Abstract

Three-scale homogenization procedure is proposed in this paper to provide estimates of the effective thermal conductivities of porous carbon-carbon textile composites. On each scale - the level of fiber tow (micro-scale), the level of yarns (meso-scale) and the level of laminate (macro-scale) - a two step homogenization procedure based on the Mori-Tanaka averaging scheme is adopted. This involves evaluation of the effective properties first in the absence of pores. In the next step, an ellipsoidal pore is introduced into a new, generally orthotropic, matrix to make provision for the presence of crimp voids and transverse and delamination cracks resulting from the thermal transformation of a polymeric precursor into the carbon matrix. Other sources of imperfections also attributed to the manufacturing processes, including non-uniform texture of the reinforcements, are taken into consideration through the histograms of inclination angles measured along the fiber tow path together with a particular shape of the equivalent ellipsoidal inclusion proposed already in (Skoček *et al.*, 2008). The analysis shows that a reasonable agreement of the numerical predictions with experimental measurements can be achieved.

*Key words:* Carbon-carbon composites, multi-scale analysis, Mori-Tanaka method, optimization, porous materials

---

## 1 Introduction

Since its introduction the Mori-Tanaka (MT) method (Mori and Tanaka, 1973) has enjoyed a considerable interest in a variety of engineering applications. These

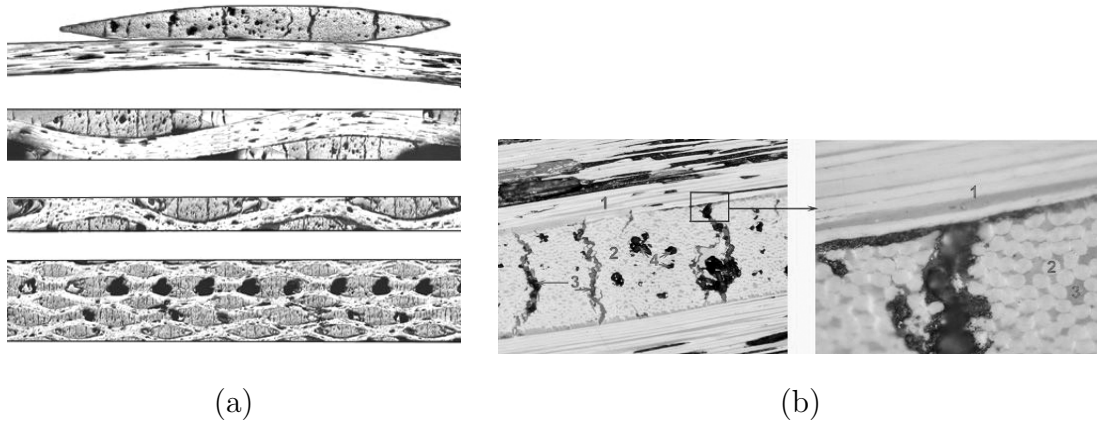


Fig. 1. Color images of a real composite system: (a) Scheme of multi-scale structural model (from top - transverse and longitudinal view of fiber tow composite, composite unit cell, composite lamina, composite plate), (b) Carbon tow microstructure showing major pores and transverse cracks.

include classical fiber matrix composites (Benveniste, 1987; Dvorak and Sejnoha, 1996), natural fiber systems (Hellmich and Ulm, 2005), or even, although to a lesser extent, typical civil engineering materials such as asphalts (Lackner *et al.*, 2005) or cement pastes (Šmilauer and Bittnar, 2006). While generally applied to modest geometries, it has also been demonstrated that the MT method may reliably assist the engineer to meet the ever growing challenge associated with the analysis of new highly complicated material systems such as textile reinforced composites (Gommers *et al.*, 1998; Huysmans *et al.*, 1998).

Recent studies addressing the behavior of imperfect carbon-carbon (C/C) textile composites (Skoček *et al.*, 2008) further promote the use of the MT method as it allows for a direct introduction of various types of imperfections, e.g. in the fiber tow path represented for example by histograms of distribution of the fiber-tow orientation angles (Košíková and Vopička, 2001). Although carbon-carbon plain weave composites belong to a progressive material systems with many applications, a relevant micromechanics model taking into account most of the geometrical details is still missing. Several appealing routes have been already offered to satisfactorily reflect commonly observed imperfections both in the woven path and through the laminate thickness developed during the manufacturing process (Zeman and Šejnoha, 2004; Skoček *et al.*, 2008). The reported works failed, however, to include one of the most important features of C/C composites illustrated in Fig. 1 - the porosity, which in real systems may exceed 30% of the overall volume.

A general awareness of the need for incorporating the porous phase in the predictions of overall response of C/C composites has been manifested in several recent works. While all microstructural details were properly identified, the actual analysis was limited to either unidirectional fiber composites represented here by individual yarns (Tsukrov *et al.*, 2005; Piat, Tsukrov, Mladenov, Verijenko, Guellali, Schnack and Hoffman, 2007; Piat, Tsukrov, Mladenov, Guellali, Ermel, Beck and Hoffman,

2007) or finite element simulations of entire laminate performed in two-dimensional (2D) environment only (Tomková *et al.*, 2008). An extension of this topic taking into consideration the characteristic three-dimensional (3D) structure of C/C textile composites is presented in this paper. The formulation given here is in the spirit of multi-scale analysis discussed in (Tomková *et al.*, 2008) combined with the application of the MT method to the prediction of effective elastic properties of C/C composite presented in (Skočec *et al.*, 2008). However, due to the constant importance of high-temperature systems with a particular role of C/C composites we consider in this paper the subject of effective thermal conductivities.

The paper is organized as follows. General description of the Mori-Tanaka method in the framework of steady state heat conduction problem is outlined in Section 2. For an extensive list of references in this subject the reader is referred to (Hatta and Taya, 1986; Benveniste *et al.*, 1990; Jeong *et al.*, 1998). Two particular issues are addressed: solution of the problem of a solitary ellipsoidal inclusion embedded into an orthotropic matrix, see e.g. (Chen and Yang, 1995), and evaluation of orientation-dependent average fields. The ordering of the remaining sections follows the concept of the assumed uncoupled multi-scale homogenization approach in which the results derived from the homogenization step on a lower scale are used as an input to the same analysis performed on the upper scale. Following (Tomková *et al.*, 2008) three particular scales are examined. The level of fiber tow evident from Fig. 1(b) is treated in Section 3 while Section 4 examines various geometrical scenarios encountered at the level of textile ply, see Fig. 1(a). Section 5 then provides the estimates of the effective thermal conductivities of the laminate and compares those with the available experimental measurements. Standard matrix notation is used throughout the paper.

## 2 Mori-Tanaka method

As illustrated in Fig. 1 both micro- (fiber tow) and meso- (textile ply) scales call for treating at minimum a three phase composite medium comprising a homogeneous matrix, a certain type of reinforcement and voids. Combining all three phases in a single homogenization step appears, however, rather inadequate owing to a considerable difference in both size and shape between the reinforcements and voids. Therefore, a two step homogenization approach is adopted in this paper. In particular, the effective properties of a composite aggregate are first found in the absence of pores followed by the second homogenization step in which the porous phase is introduced into a new homogenized matrix.

It is therefore sufficient to consider a two-phase composite medium with the heterogeneities (reinforcements or voids) having in general a certain orientation distribution. Let this composite be subjected on its outside boundary  $\Gamma$  to a homogeneous temperature boundary condition defined as (Benveniste *et al.*, 1990; Tomková *et al.*,

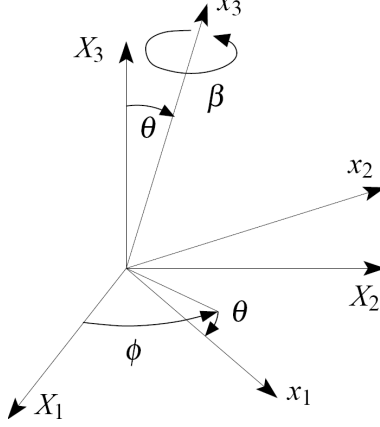


Fig. 2. Local coordinate system and definition of the Euler angles.

2008)

$$\theta(\mathbf{X}) = \mathbf{H}^T \mathbf{X} \quad \text{on } \Gamma, \quad (1)$$

where  $\mathbf{H}$  represents the macroscopically uniform temperature gradient vector and  $\mathbf{X}$  are the components of the assigned (fixed, global) Cartesian coordinate system, Fig. 2. The volume average of the local constitutive equation written in the local  $\mathbf{x}$ -coordinate system is then provided by

$$\mathbf{q}_r^x = -\boldsymbol{\chi}_r^x \mathbf{h}_r^x, \quad (2)$$

where  $\mathbf{q}_r$  is the volume average of the local heat flux in the phase  $r$  ( $r = 1, 2$  with  $r = 1$  reserved for the matrix phase) and  $\boldsymbol{\chi}_r$  is the corresponding thermal conductivity matrix [ $\text{Wm}^{-1}\text{K}^{-1}$ ]. Also note that  $\mathbf{x} \equiv \mathbf{X}$  for the matrix phase.

Next, in the context of the Mori-Tanaka method, consider a certain auxiliary transformation problem where a single heterogeneity in an infinite matrix is replaced by an equivalent inclusion of the same shape and orientation but having the material properties of the matrix phase. In the Mori-Tanaka mean field theory the mutual interaction of individual heterogeneities is taken into account by loading such a configuration at infinity by the average temperature gradient in the matrix  $\mathbf{h}_1$ , see e.g. (Benveniste, 1987; Benveniste *et al.*, 1990) for further details. The local temperature gradient in the inclusion is then expressed as

$$\mathbf{h}_2^x = \mathbf{h}_1^x + (\mathbf{S}\mathbf{h}^*)^x, \quad (3)$$

where  $\mathbf{h}^*$  represents a certain transformation temperature gradient introduced in the homogeneous, generally anisotropic, matrix to give the same local fluxes as in the composite. Note that the second order tensor  $\mathbf{S}$  and the vector  $\mathbf{h}^*$  are analogous to the Eshelby tensor and transformation strain known from the solution of the Eshelby equivalent inclusion problem in elasticity (Eshelby, 1957) (hereafter, we shall quote the ‘‘Eshelby problem’’ whenever referring to a general transformation inclusion problem). Recall that in the MT scheme the  $\mathbf{S}$  tensor is a function of the matrix material parameters and the shape of the inclusion. Combining Eqs. (2)

and (3) for the heterogeneity and equivalent inclusion then gives

$$\mathbf{q}_2^x = -\boldsymbol{\chi}_2^x \mathbf{h}_2^x = -\boldsymbol{\chi}_1^x (\mathbf{h}_2^x - (\mathbf{h}^*)^x), \quad (4)$$

so that

$$(\mathbf{h}^*)^x = (\boldsymbol{\chi}_1^x)^{-1} (\boldsymbol{\chi}_1^x - \boldsymbol{\chi}_2^x) \mathbf{h}_2^x. \quad (5)$$

Next, substitute Eq. (5) into (3) to get

$$\mathbf{h}_2^x = \mathbf{h}_1^x + \mathbf{S}^x (\boldsymbol{\chi}_1^x)^{-1} (\boldsymbol{\chi}_1^x - \boldsymbol{\chi}_2^x) \mathbf{h}_2^x, \quad (6)$$

and finally

$$\mathbf{h}_2^x = [\mathbf{I} - \mathbf{S}^x (\boldsymbol{\chi}_1^x)^{-1} (\boldsymbol{\chi}_1^x - \boldsymbol{\chi}_2^x)]^{-1} \mathbf{h}_1^x = \mathbf{T}_2^x \mathbf{h}_1^x, \quad (7)$$

where  $\mathbf{I}$  is the identity matrix and the matrix  $\mathbf{T}_2$  is referred to as the partial concentration factor.

Suppose that the heterogeneity possess a certain orientation described by the orientation distribution function  $g(\phi, \theta, \beta)$  with  $\phi, \theta$  and  $\beta$  being the Euler angles. A particular form of  $g$  for plain weaved composites is given later in Section 4. In general, following (Jeong *et al.*, 1998), the overall average temperature gradient for a two-phase composite with an orientation-dependent inclusion given in the global  $\mathbf{X}$ -coordinate system then attains the form

$$\langle \mathbf{h} \rangle = c_1 \mathbf{h}_1 + c_2 \langle \langle \mathbf{h}_2 \rangle \rangle, \quad (8)$$

where  $c_r$  is the volume fraction of the phase  $r$ ,  $\langle \rangle$  stands for the volumetric averaging and the double brackets  $\langle \langle \rangle \rangle$  denote averaging over all possible orientations. The vector  $\mathbf{h}_2$  in Eq. (8) follows from standard transformation of coordinates so that

$$\mathbf{X} = \mathbf{Q} \mathbf{x} \quad \text{and} \quad \mathbf{h}_2 = \mathbf{Q} \mathbf{h}_2^x = \mathbf{Q} \mathbf{T}_2^x \mathbf{Q}^\top \mathbf{h}_1 = \mathbf{T}_2 \mathbf{h}_1. \quad (9)$$

A specific form of the transformation matrix  $\mathbf{Q}$  consistent with Fig. 2<sup>1</sup> reads

$$\mathbf{Q} = \begin{bmatrix} \cos \phi \cos \theta \cos \beta - \sin \phi \sin \beta & \sin \phi \cos \theta \cos \beta + \cos \phi \sin \beta & -\sin \theta \cos \beta \\ -\cos \phi \cos \theta \sin \beta - \sin \phi \cos \beta & -\sin \phi \cos \theta \sin \beta + \cos \phi \cos \beta & \sin \theta \sin \beta \\ \cos \phi \sin \theta & \sin \phi \sin \theta & \cos \theta \end{bmatrix}.$$

Next, suppose that the local temperature gradient  $\mathbf{h}_2$  is expressed in terms of the prescribed macroscopically uniform temperature gradient  $\mathbf{H} = \langle \mathbf{h} \rangle$  as

$$\mathbf{h}_2 = \mathbf{A}_2 \mathbf{H}, \quad (10)$$

<sup>1</sup> Note that so-called "x<sub>2</sub> convention" is used; i.e. a conversion into a new coordinates system follows three consecutive steps. First, the rotation of angle  $\phi$  around the original  $X_3$  axis is done. Then, the rotation of angle  $\theta$  around the new  $x_2$  axis is followed by the rotation of angle  $\beta$  around the new  $x_3$  axis to finish the conversion.

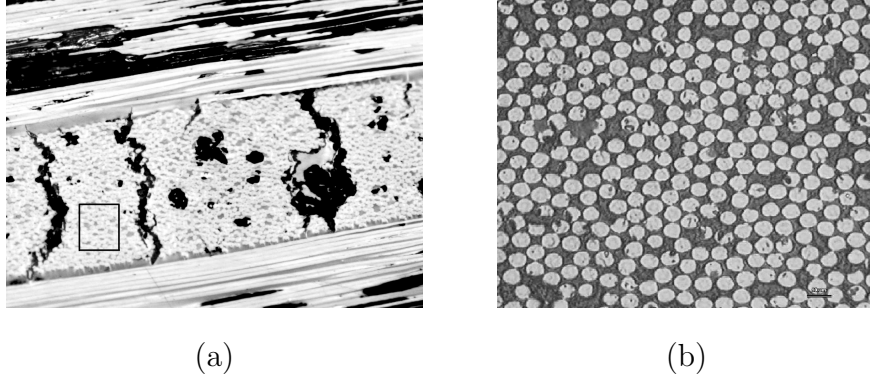


Fig. 3. Homogenization on micro-scale: (a) fiber tow composite, (b) fiber-matrix composite where the matrix  $\mathbf{A}_2$  is termed the concentration factor (Benveniste *et al.*, 1990; Jeong *et al.*, 1998) for the heterogeneity. Clearly, the orientation average of  $\mathbf{h}_2$  then follows from

$$\langle\langle \mathbf{h}_2 \rangle\rangle = \langle\langle \mathbf{T}_2 \rangle\rangle \mathbf{h}_1 = \langle\langle \mathbf{A}_2 \rangle\rangle \mathbf{H}, \quad (11)$$

which, together with Eqs. (7)–(9) gives

$$\langle\langle \mathbf{A}_2 \rangle\rangle = \langle\langle \mathbf{T}_2 \rangle\rangle [c_1 \mathbf{I} + c_2 \langle\langle \mathbf{T}_2 \rangle\rangle]^{-1}. \quad (12)$$

Combining Eqs. (8) and (11) further gives

$$c_1 \mathbf{h}_1 = [\mathbf{I} - c_2 \langle\langle \mathbf{A}_2 \rangle\rangle] \mathbf{H}. \quad (13)$$

In analogy to Eq. (8), the volume average of the overall heat flux is provided by

$$\langle \mathbf{q} \rangle = c_1 \mathbf{q}_1 + c_2 \langle\langle \mathbf{q}_2 \rangle\rangle. \quad (14)$$

Next, define an overall conductivity matrix  $\boldsymbol{\chi}$  in the fixed coordinate system  $\mathbf{X}$  and write Eq. (14) as

$$\boldsymbol{\chi} \mathbf{H} = c_1 \boldsymbol{\chi}_1 \mathbf{h}_1 + c_2 \langle\langle \boldsymbol{\chi}_2 \mathbf{h}_2 \rangle\rangle. \quad (15)$$

Introducing Eqs. (10) and (13) into Eq. (15) finally provides

$$\boldsymbol{\chi} = \boldsymbol{\chi}_1 + c_2 [\langle\langle \boldsymbol{\chi}_2 \mathbf{A}_2 \rangle\rangle - \boldsymbol{\chi}_1 \langle\langle \mathbf{A}_2 \rangle\rangle]. \quad (16)$$

Particular forms of the homogenized matrix  $\boldsymbol{\chi}$  will be now given for individual micromechanics problems.

### 3 Micro-scale

In the first step of the proposed multi-scale homogenization scheme we consider a single filament (fiber tow) of a plain weave carbon fabric Hexcel 1/1 bonded to a

carbon matrix, Fig. 3(a). Each filament contains about 6000 carbon fibers T800H and significant amount of transverse cracks and voids resulting in a porosity of more than 10% (Tomková and Košková, 2004; Tomková *et al.*, 2008). While the matrix phase, which essentially corresponds to a glassy carbon, is assumed isotropic the carbon fiber possess a transverse isotropy with the value of longitudinal thermal conductivity considerably exceeding the one in the transverse direction. The phase thermal conductivities are listed in Table 1. Considerable difference in the size of the two types heterogeneities (fibers and pores) readily suggests a two step homogenization procedure to predict the effective properties of the fiber tow as discussed next.

Table 1

Material parameters of individual phases (TORAYCA, 2008; Ohlhorst, 1997)

| Material              | Thermal conductivity<br>[Wm <sup>-1</sup> K <sup>-1</sup> ] |
|-----------------------|---|
| Carbon fibers         | (0.35, 0.35, 35)  |
| Carbon matrix         | 6.3   |
| Voids filled with air | 0.02  |

### 3.1 Effective conductivities of fiber matrix composites

Fig. 3(b) shows a representative section of the fiber matrix composite taken from the fiber tow in Fig. 3(a). Based on our previous studies (Zeman and Šejnoha, 2001; Šejnoha and Zeman, 2002; Šejnoha *et al.*, 2004, to cite a few) such a composite can be quantified as ergodic, statistically homogeneous with a random distribution of fibers having the volume fraction of approximately 50%. In the MT scheme the effective properties follow from the solution of an auxiliary problem where an infinite cylinder of a circular cross-section with semi-axes  $\xi_1 \rightarrow \infty$ ,  $\xi_2 = \xi_3$  (the  $x_1$  axis assumed in the fiber direction) is embedded into an infinite isotropic matrix. In this particular case the effective thermal conductivity matrix given by Eq. (16) simplifies as

$$\boldsymbol{\chi} = \boldsymbol{\chi}_1 + c_2 (\boldsymbol{\chi}_2 - \boldsymbol{\chi}_1) \mathbf{A}_2, \quad (17)$$

where

$$\mathbf{A}_2 = \mathbf{T}_2 [c_1 \mathbf{I} + c_2 \mathbf{T}_2]^{-1} \quad \text{and} \quad \mathbf{T}_2 = [\mathbf{I} - \mathbf{S} \boldsymbol{\chi}_1^{-1} (\boldsymbol{\chi}_1 - \boldsymbol{\chi}_2)]^{-1}. \quad (18)$$

An explicit form of  $\mathbf{S}$  for this particular case of aligned circular fibers in an isotropic matrix is available in (Hatta and Taya, 1986).

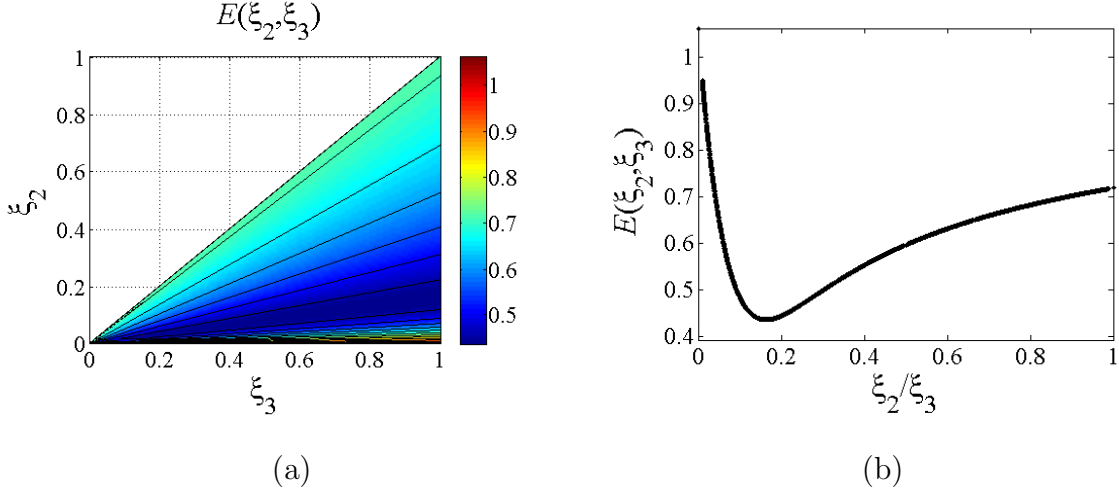


Fig. 4. Evolution of the objective function as a function of the aspect ratio

### 3.2 Effective conductivities of homogenized porous matrix

Having derived the effective properties of the fiber matrix composite we proceed with the second homogenization step to account for the porous phase. As evident in Fig. 3(a), several distinct shapes of voids can be identified. It is certainly out of the question to treat each void separately. Therefore, in the present study, they are all combined into a single equivalent inclusion resembling an elliptic cylinder. Here, the cylinder is embedded into a transversely isotropic matrix. However, since the  $S_{11}$  component of  $\mathbf{S}$  is equal to zero, the solution of an elliptic cylinder in an isotropic matrix summarized in (Hatta and Taya, 1986) is again applicable. This results in the same form of estimate of the effective conductivity matrix  $\chi$  as given by Eq. (17).

Nevertheless, there is still one open problem associated with the shape of the elliptical cross-section. Clearly, since the equivalent inclusion represents all possible shapes of voids, it can hardly be determined directly from the images of real composites such as the one in Fig. 3(a). Instead, to solve this particular problem, we exploited the results available from the finite element (FE) simulations carried out in (Tomková *et al.*, 2008). In particular, the optimal aspect ratio  $\xi_2/\xi_3$  ( $\xi_1 \rightarrow \infty$ ) of the elliptical cross-section was found by matching the effective material properties derived from both the MT method and FE solutions. Fig. 4 shows a variation of the objective function  $E$

$$E(\xi_2, \xi_3) = \left[ \sum_{i=1}^3 \left( \chi_{ii}^{\text{FEM}} - \chi_{ii}^{\text{MT}}(\xi_2, \xi_3) \right)^2 \right]^{1/2}.$$

The resulting effective thermal conductivities provided by the proposed two-step homogenization scheme are stored in Table 2 (Note that the fiber volume fraction  $c_{\text{fiber}}$



was estimated from Fig. 3(b), while the volume fraction of voids  $c_{void} = V_{void}/V_{tow}$  stands for the total volume of voids in the fiber tow in Fig. 3(a)). It also clearly shows a significance in properly choosing the shape of the cross-section of the equivalent elliptic cylinder. Thereby, to make the analysis more robust, an empirical relation between the observed porosity and representative equivalent inclusion is needed. This particular topic enjoys our current research interest.

Table 2  
Effective thermal conductivities of the fiber tow

| Material                                   | Equivalent inclusion  |                          | Thermal conductivity<br>[Wm <sup>-1</sup> K <sup>-1</sup> ] |
|--|-----------------------|--------------------------|---|
|  | fiber ( $c_{fiber}$ ) | void ( $c_{void}$ )      |   |
| Fiber-matrix composite                     | $\infty, 1, 1$ (0.55) |                          | 22.09, 2.14, 2.14   |
| Porous fiber-tow<br>(optimal aspect ratio) | →                     | $\infty, 1, 1$ (0.12)    | 19.44, 1.54, 1.54   |
|  |                       | $\infty, 1, 10$ (0.12)   | 19.44, 1.02, 1.63   |
|  |                       | $\infty, 1.6, 10$ (0.12) | <b>19.44, 1.12, 1.85</b>                                    |

#### 4 Meso-scale

While unidirectional fiber matrix composites reviewed in the previous section have been of a general interest since some fifty years ago, composite systems with a formidable textile texture have received more attention from both academic and industrial communities only recently.

This section examines, at least from the geometrical point of view, the most simple representative - a plain weave textile composite. One of the earliest known computational models focusing on actual geometry of the textile ply is developed in (Kuhn and Charalambides, 1999). A three-dimensional view with a typical cross-section are plotted in Fig. 5(a)(b). The idealized geometry of this model assumes the centerlines of the warp and fill systems of tows to be described by a simple trigonometric form

$$c(x) = \frac{b}{2} \sin\left(\frac{\pi x}{a}\right). \quad (19)$$

Although tempting, a direct application of this model is precluded by a number of imperfections and irregularities present in real systems as illustrated in Fig. 1. These include a non-uniform waviness, mutual shift of individual yarns from layer to layer and most importantly a non-negligible porosity. Unlike finite element simulations which enable incorporating most of these imperfections directly through the formulation of a certain statistically equivalent periodic unit cell (Zeman and Šejnoha, 2004; Šejnoha and Zeman, 2008), the MT method has only limited means which are,

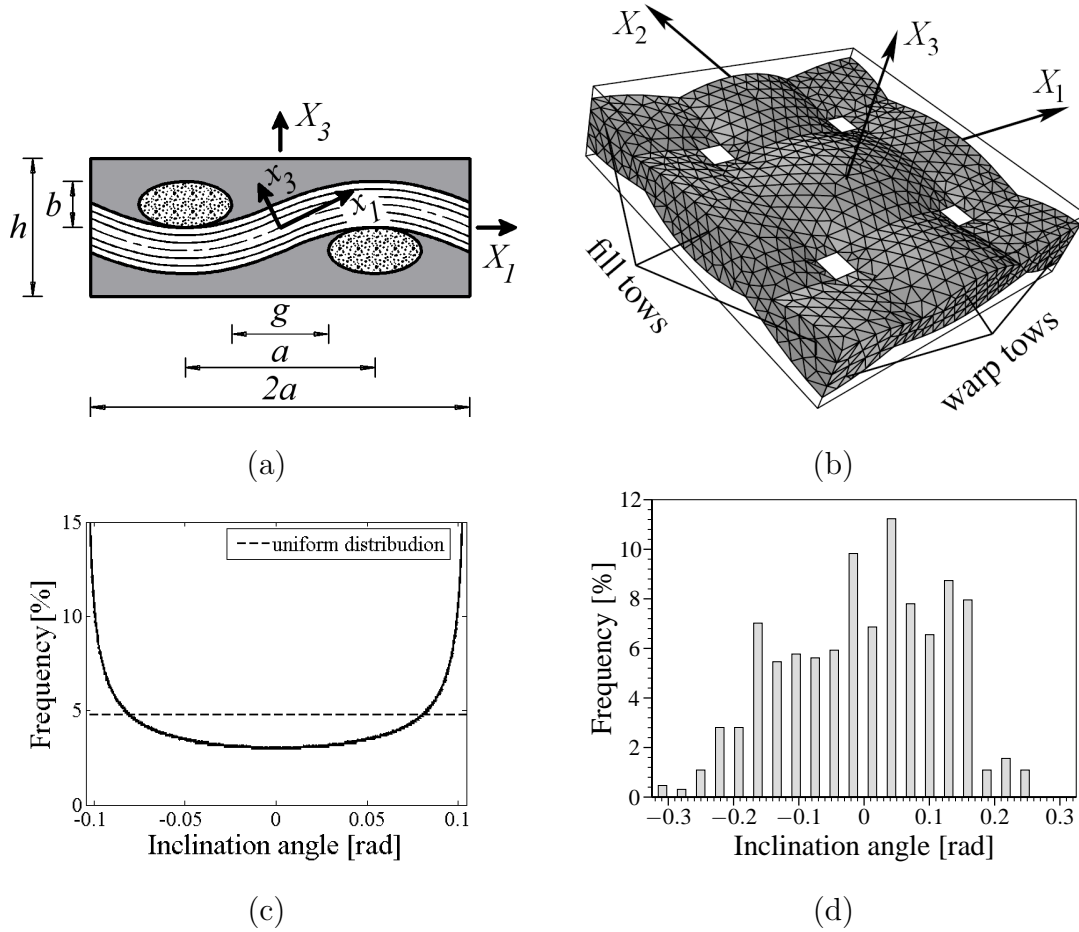


Fig. 5. Ideal periodic unit cell: (a) cross-section, (b) three-dimensional view, (c) approximate distribution of inclination angles, (d) example of a real distribution of inclination angles

nevertheless, still sufficient when quick estimates of the effective “bulk” response is needed. These will be discussed next in the framework of the two-step homogenization procedure examined already in the previous section.

#### 4.1 Effective conductivities of plain weave textile composite ply

Consider a simple plain weave fabric ply in the absence of porous ply. At this level, the carbon fiber tow is treated as a homogeneous phase with known material properties bonded again to an isotropic carbon matrix. In order to address the influence of various geometrical flaws, the approach proposed in (Skoček *et al.*, 2008) is adopted. This involves:

- (1) determination of an ideal geometrical model to assess the volume fraction of the fiber tow
- (2) determination of the optimal shape of an equivalent ellipsoidal inclusion sub-

- stituting the fiber tow in the solution of the Eshelby problem
- (3) proper evaluation of orientation dependent quantities from Eq. (16) to account for a non-uniform waviness along the fiber tow path

#### 4.1.1 Ideal geometrical model - Fig. 5(b)

The three-dimensional geometrical model adopted in the present work (Kuhn and Charalambides, 1999) is characterized by four parameters: the tow wavelength  $2a$ , the tow height  $b$ , tow spacing  $g$  and the layer thickness  $h$ . To formulate one particular “ideal” representative, a tedious image analysis of a number of sections of a real textile ply such as the one in Fig. 1(a<sub>1</sub>) was carried out. The averages of the basic geometrical parameters presented in Table 3 were used to construct the required geometrical model.

Table 3  
Quantification of PUC1 parameters (Tomková, 2004)

| Statistics [ $\mu m$ ] | $a$  | $h$ | $b$ | $g$ |
|------------------------|------|-----|-----|-----|
| Average                | 2250 | 300 | 150 | 400 |
| Standard deviation     | 155  | 50  | 20  | 105 |

#### 4.1.2 Optimal shape of the equivalent ellipsoidal inclusion

An extensive numerical study was performed in (Skočec *et al.*, 2008) to conceive how the Mori-Tanaka predictions are influenced by a “random” deviation of basic geometrical parameters of real systems from their ideal representative introduced in the previous section. The results revealed a certain correlation between the model parameters and “optimal” shape of an equivalent ellipsoidal inclusion characterized by three semi-axes  $\xi_1, \xi_2, \xi_3$ . When setting  $\xi_1 = 1$  (recall that the Eshelby solution depends only on the mutual ratio of the ellipsoid semi-axes), it was concluded that the  $\xi_2$  parameter is strongly correlated with  $g/a$  ratio, while it is almost independent of  $b/a$  value. An analogous trend could be observed between  $\xi_3$  and  $b/a$  parameter. This led to following semi-empirical formulas employed also in this study

$$\xi_2 \approx 1 - \frac{3g}{a}, \quad \xi_3 \approx \frac{1}{10} - \frac{b}{3a}, \quad (20)$$

where the necessary parameters  $a, b, g$  are available from Table 3.

Remind, however, that these relations were originally derived to match effective elastic properties. To either confirm or displace their validity in the solution of heat conduction problem we further assumed an equivalent inclusion in the form of an infinite elliptic cylinder with elliptical cross-section estimated directly from actual cross-section of tows in the representative model giving

$$\xi_1 = \infty, \quad \xi_2 = 12.3, \quad \xi_3 = 1. \quad (21)$$

### 4.1.3 Orientation averaging

There are three distinct routes available in this study to reflect the variation of the inclination angle along the fiber tow path. If we consider directly the simplified geometrical model in Fig. 5(b), the joint probability density function  $g(\phi, \theta, \beta)$  results from the harmonic shape of the centerline as described by Eq. (19). Applying the change of variable formula (Rektorys, 1994, Section 33.9), we obtain after some algebra the expression of the probability density in the form

$$g(\phi, \theta, \beta) = \begin{cases} \frac{2a}{\pi} \frac{1 + \tan^2(\theta)}{\sqrt{b^2\pi^2 - 4a^2 \tan^2(\theta)}} & \text{if } \phi = 0, \beta = 0 \text{ and } -\alpha \leq \theta \leq \alpha, \\ 0 & \text{otherwise,} \end{cases}$$

where

$$\alpha = \arctan\left(\frac{b\pi}{2a}\right).$$

Assuming simply a uniform distribution of inclination angles the joint probability density function attains the form

$$g(\phi, \theta, \beta) = \begin{cases} \frac{1}{2\alpha} & \text{if } \phi = 0, \beta = 0 \text{ and } -\alpha \leq \theta \leq \alpha, \\ 0 & \text{otherwise.} \end{cases}$$

Both functions are plotted in Fig. 5(c) for comparison. In this study, the latter function was adopted for simplicity. Next, let  $\mathbf{D}$  represents an orientation dependent quantity in Eq. (16)

$$\langle\langle \mathbf{D} \rangle\rangle = \langle\langle \chi_2 \mathbf{A}_2 \rangle\rangle - \chi_1 \langle\langle \mathbf{A}_2 \rangle\rangle, \quad (22)$$

written, for the warp system, as

$$\langle\langle \mathbf{D}^{\text{warp}} \rangle\rangle = \int_{-\alpha}^{\alpha} g(\phi, \theta, \beta) \mathbf{D}(0, \theta, 0) d\theta, \quad (23)$$

and similarly for the fill system we get

$$\langle\langle \mathbf{D}^{\text{fill}} \rangle\rangle = \int_{-\alpha}^{\alpha} g(\phi, \theta, \beta) \mathbf{D}\left(\frac{\pi}{2}, \theta, 0\right) d\theta. \quad (24)$$

Finally, following (Skoček *et al.*, 2008), the resulting homogenized stiffness matrix given by Eq. (16) then becomes

$$\boldsymbol{\chi} = \boldsymbol{\chi}_1 + \frac{c_2}{2} \left[ \langle\langle \mathbf{D}^{\text{warp}} \rangle\rangle + \langle\langle \mathbf{D}^{\text{fill}} \rangle\rangle \right], \quad (25)$$

One may also suggest to model the plain weave fabric as a three-phase composite with warp and fill systems of yarns being considered as two distinct phases. The homogenized conductivity matrix then attains a slightly different form

$$\boldsymbol{\chi} = \boldsymbol{\chi}_1 + \frac{c_2}{2} \left[ \langle\langle \boldsymbol{\chi}^{\text{warp}} \mathbf{A}^{\text{warp}} + \boldsymbol{\chi}^{\text{fill}} \mathbf{A}^{\text{fill}} \rangle\rangle - \boldsymbol{\chi}_1 \langle\langle \mathbf{A}^{\text{warp}} + \mathbf{A}^{\text{fill}} \rangle\rangle \right], \quad (26)$$

where

$$\mathbf{A}^{\text{warp}} = \mathbf{T}^{\text{warp}} \left[ c_1 \mathbf{I} + \frac{c_2}{2} (\mathbf{T}^{\text{warp}} + \mathbf{T}^{\text{fill}}) \right]^{-1}, \quad \mathbf{T}^{\text{warp}} = \mathbf{T}^{\text{warp}}(0, \theta, 0), \quad (27)$$

$$\mathbf{A}^{\text{fill}} = \mathbf{T}^{\text{fill}} \left[ c_1 \mathbf{I} + \frac{c_2}{2} (\mathbf{T}^{\text{warp}} + \mathbf{T}^{\text{fill}}) \right]^{-1}, \quad \mathbf{T}^{\text{fill}} = \mathbf{T}^{\text{fill}}\left(\frac{\pi}{2}, \theta, 0\right). \quad (28)$$

However, the differences in predictions provided by Eqs. (25) and (26) are, as seen in Table 4, negligible.

Improvements when compared to the assumed ideal geometry are contained in the third route which allows us to introduce the non-uniform waviness and to some extent also the mutual shift of individual layers by utilizing histograms of inclination angles shown in Fig. 5(d). These are derived from centerlines of individual fiber tows described in detail in (Vopička, 2004). Representing the joint probability density function by these histograms, the contribution to the effective conductivity matrix, e.g. from the warp direction Eq. (23), reads

$$\langle\langle \mathbf{D}^{\text{warp}} \rangle\rangle = \sum_{i=1}^m p_i \mathbf{D}(0, \theta_i, 0), \quad (29)$$

where  $m$  denotes the number of sampling values. The discrete angles  $\theta_i$  and probabilities  $p_i$  follow directly from the image analysis data. Eleven such histograms associated with several sections measured along individual plies were considered. The resulting averages together with the estimates provided by the simplified distribution functions are summarized in Table 4. For the solution of the Eshelby problem of an ellipsoidal inclusion in an isotropic matrix we refer the interested reader to (Hatta and Taya, 1986; Jeong *et al.*, 1998).

#### 4.2 Effective conductivities of homogenized porous matrix

When carefully observing Fig. 1(a<sub>4</sub>) we identify three more or less periodically repeating geometries further displayed in Fig. 6. These segments readily confirm the need for the proposed two step homogenization procedure as the ideal representative plotted in Figs. 6(a)(b) (already analyzed in the previous section) cannot be used to represent the entire composite. Instead, the second homogenization step is required to account for the presence of large vacuoles evident from Figs. 6(c)-(f).

Owing to the orthogonal arrangement of tows in the ideal (representative) model the new homogenized matrix employed in the second homogenization step is no longer isotropic. Thereby, the Eshelby solutions used so far are not directly applicable. Instead, the  $\mathbf{S}$  tensor is found by imagining an equivalent ellipsoidal inclusion in an infinite matrix being orthotropic. The corresponding Laplace equation governing

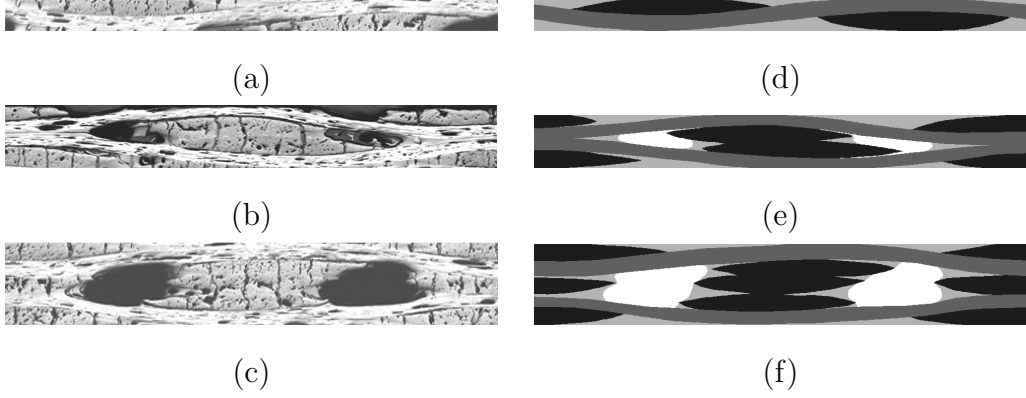


Fig. 6. Homogenization on meso-scale: (a)-(b) PUC1 representing carbon tow-carbon matrix composite, (c)-(d) PUC2 with vacuoles aligned with delamination cracks due to slip of textile plies, (e)-(f) PUC3 with extensive vacuoles representing the parts with textile reinforcement reduction due to bridging effect in the middle ply

the steady state heat conduction problem is provided by

$$\chi_1 \frac{\partial^2 \theta}{\partial X_1^2} + \chi_2 \frac{\partial^2 \theta}{\partial X_2^2} + \chi_3 \frac{\partial^2 \theta}{\partial X_3^2} = 0. \quad (30)$$

Introducing the following substitutions

$$X_1 = \sqrt{\chi_1} \tilde{X}_1; \quad X_2 = \sqrt{\chi_2} \tilde{X}_2; \quad X_3 = \sqrt{\chi_3} \tilde{X}_3, \quad (31)$$

allows us to convert Eq. (30) into

$$\frac{\partial^2 \theta}{\partial \tilde{X}_1^2} + \frac{\partial^2 \theta}{\partial \tilde{X}_2^2} + \frac{\partial^2 \theta}{\partial \tilde{X}_3^2} = 0, \quad (32)$$

which eventually leads to

$$S_{ii} = \frac{\xi_1 \xi_2 \xi_3}{2\sqrt{\chi_1 \chi_2 \chi_3}} \int_0^\infty \frac{1}{((\xi_i)^2/\chi_i + s) \Delta s} ds, \quad (33)$$

where

$$\Delta s = \sqrt{((\xi_1)^2/\chi_1 + s) ((\xi_2)^2/\chi_2 + s) ((\xi_3)^2/\chi_3 + s)}. \quad (34)$$

These equations then formally resemble those derived for the case of an isotropic matrix. The solution of Eq. (33) given in the form of elliptic integrals is available in (Jeong *et al.*, 1998).

A simple example of an isotropic void (ellipsoidal inclusion with  $\boldsymbol{\xi} = (1, 1.5, 2)$ ,  $\chi^v = 0.2$ ) surrounded by an orthotropic matrix ( $\chi_{11}^m = 20$ ,  $\chi_{22}^m = 1$ ,  $\chi_{33}^m = 2$ ) was considered to acknowledge correctness of Eq. (33). Fig. 7 compares the MT predictions with the finite element results found for a hexagonal arrangement of voids under periodic boundary conditions (Tomková *et al.*, 2008).

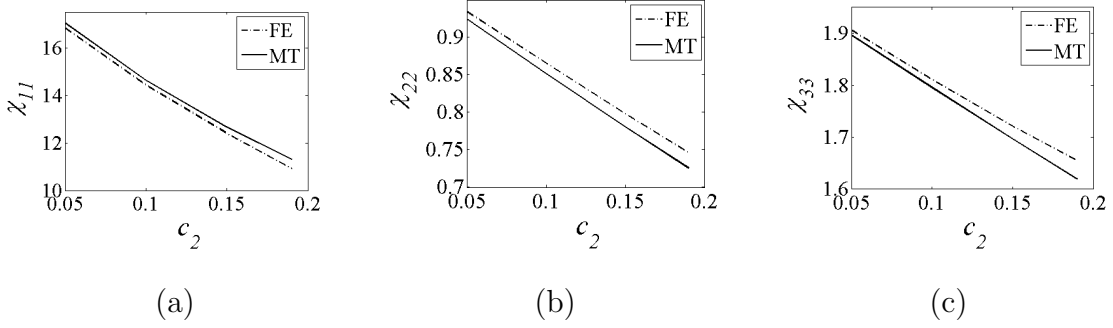


Fig. 7. Case study: effective conductivities in  $[\text{Wm}^{-1}\text{K}^{-1}]$  as a function of the volume fraction of the porous phase

With these encouraging results at hand we proceeded with the analysis of real systems. Unlike the micro-scale, the method of observation and measuring tools provided by the LUCIA G software (LIM, 2008) were utilized here to approximate the shape of individual vacuoles in Figs. 6(c)-(f). Since only two-dimensional (2D) images were supplied, the voids were assumed to be well approximated by an oblate spheroid defined in Table 5 for both types of representative periodic unit cells in Figs. 6(d)(f). To estimate the mesoscopic effective properties the voids were introduced into the homogenized matrix derived in the 1st homogenization step by combining Eqs. (25) and (29) (the last two columns in Table 4).

A word of caution, however, is appropriate when dealing with 2D images only. While the shape of the inclusion acquired from 2D images may play a minor role in final predictions of the effective properties, the volume fraction of a relevant heterogeneity also estimated from 2D images may prove much more important. This is documented in Table 4 listing the predicted effective properties of a plain weave fabric free of pores for two different volume fractions of the homogenized fiber tow. The volume fraction 0.53 corresponds to a representative 3D meso-structure in Fig. 5(b), whereas the value of 0.78 follows from the corresponding 2D image in Fig. 6(b).

Table 4

Effective thermal conductivities of a plain weave fabric without porosity in  $[\text{Wm}^{-1}\text{K}^{-1}]$

| Method   | Fiber tow<br>volume<br>fraction | Thermal conductivity |             |           |        |                |             |
|----------|---------------------------------|----------------------|-------------|-----------|--------|----------------|-------------|
|          |                                 | Eqs. (25)&(23)       |             | Eq. (26)  |        | Eqs. (25)&(29) |             |
|          |                                 | warp/fill            | trans.      | warp/fill | trans. | warp/fill      | trans.      |
| MT       | 0.53                            | 8.18                 | 3.08        | 7.93      | 3.07   | <b>8.14</b>    | <b>3.16</b> |
| Eq. (20) | 0.78                            | 9.23                 | 2.37        | 8.68      | 2.34   | 9.18           | 2.48        |
| MT       | 0.53                            | 8.35                 | 2.94        | 8.26      | 2.92   | 8.31           | 3.02        |
| Eq. (21) | 0.78                            | 9.35                 | 2.30        | 9.15      | 2.27   | 9.29           | 2.42        |
| 3D FEM   | 0.53                            | <b>8.13</b>          | <b>3.18</b> | -         |        |                |             |

The mesoscopic effective conductivities derived for individual geometries in Fig. 6 are summarized in Table 5 for both volume fractions of the fiber tow. Note that the results corresponding to a representative model denoted as PUC1 are essentially those stored in Table 4 which of course served as a point of departure for the 2nd homogenization step performed for models PUC2 and PUC3.

Table 5

Effective thermal conductivities of the porous textile plies and laminates in  $[\text{Wm}^{-1}\text{K}^{-1}]$

| Fiber tow in 1st step |          | Void |             |            | Thermal conductivity |             |
|-----------------------|----------|------|-------------|------------|----------------------|-------------|
| vol. frac.            | shape    | PUC  | shape       | vol. frac. | warp/fill            | transverse  |
| 0.53                  | Eq. (20) | PUC2 | 3; 3; 1     | 0.07       | <b>7.40</b>          | <b>2.75</b> |
|                       |          | PUC3 | 1.6; 1.6; 1 | 0.15       | <b>6.44</b>          | <b>2.51</b> |
|                       | Eq. (21) | PUC2 | 3; 3; 1     | 0.07       | 7.55                 | 2.63        |
|                       |          | PUC3 | 1.6; 1.6; 1 | 0.15       | 6.57                 | 2.40        |
| 0.78                  | Eq. (20) | PUC2 | 3; 3; 1     | 0.07       | 8.32                 | 2.18        |
|                       |          | PUC3 | 1.6; 1.6; 1 | 0.15       | 7.21                 | 1.99        |
|                       | Eq. (21) | PUC2 | 3; 3; 1     | 0.07       | 8.42                 | 2.13        |
|                       |          | PUC3 | 1.6; 1.6; 1 | 0.15       | 7.29                 | 1.95        |

Table 6

Effective thermal conductivities of the laminate  $[\text{Wm}^{-1}\text{K}^{-1}]$

| Method                                  | Fiber tow in 1st step |                 | Thermal conductivity |             |
|---|-----------------------|-----------------|----------------------|-------------|
|   | shape                 | volume fraction | warp/fill            | transverse  |
| MT<br>(histograms)                      | Eq. (20)              | 0.53            | <b>7.26</b>          | <b>2.76</b> |
|   |                       | 0.78            | 8.15                 | 2.18        |
| MT<br>(histograms)                      | Eq. (21)              | 0.53            | 7.40                 | 2.64        |
|   |                       | 0.78            | 8.25                 | 2.13        |
| 2D FEM (Tomková <i>et al.</i> , 2008)   | -                     | 0.78            | <i>8.67</i>          | <i>1.66</i> |
| Measured (Kubičár <i>et al.</i> , 2002) | -                     | -               | <i>10</i>            | <i>1.6</i>  |

## 5 Macro-scale

The final, clearly the most simple, step requires construction of the homogeneous laminated plate. The stacking sequence of individual periodic unit cells complies with that observed for the actual composite sample (Tomková *et al.*, 2008, Fig. 2), see also Fig. 1(a<sub>4</sub>) identifying the PUC1/PUC2/PUC3/PUC1 stacking sequence.



While in-plane conductivities (warp/fill directions) were found from a simple arithmetic rule of mixture, the out-of-plane (transverse) conductivity followed from the inverse (geometric) rule of mixture. The resulting effective thermal conductivities are available in Table 6 comparing the MT predictions and experimental measurements presented in (Kubičár *et al.*, 2002). The FEM results obtained from 2D simulations in (Tomková *et al.*, 2008) are provided for additional comparison. Note that the highlighted (bold font) values of thermal conductivities stored in Tables 2–6 follow from what we would call an optimal or the most appropriate approach.

## 6 Discussion and conclusions

In order to realistically model complex plain weave textile laminates with three-dimensional, generally non-uniform texture of the reinforcements and significant amount of porosity we advocate to consider at least three levels of hierarchy - the level of fiber tow, the level of yarns and the level of laminate. On each level different resolutions of microstructural details are considered on individual scales for the formulation of an adequate representative model. The desired macroscopic effective properties of the laminate are then estimated with regard to two basic objectives:

- to reflect the three-dimensional character of the composite at all scales,
- to predict the effective conductivities as efficiently as possible.

Unlike computationally tedious and extensive 3D finite element simulations the Mori-Tanaka averaging scheme appears as a reasonable candidate to comply with both objectives. Not only the fully explicit format of this method but a simple extension of the Eshelby problem, at least in the case of the solution of heat conduction problem, to generally orthotropic reference medium (homogenized composite free of pores in our particular case) favors this technique.

In this study, the hierarchical character of the analysis is presented in a totally uncoupled format. Therefore, each level is treated entirely independently purely upscaling the results from a lower to higher scale for subsequent calculations. An “optimal” procedure, which attempts to accommodate various sources of imperfections observed in real systems is accompanied by several modifications involving mainly the meso-scale.

Based on our previous study of effective elastic properties (Zeman and Šejnoha, 2004; Skoček *et al.*, 2008) it was expected that at this level the “best” estimates of the effective conductivities would follow from the application of Eq. (20) to determined the shape of an equivalent inclusion for the fiber tow representation and histograms of fiber inclination angle to proceed with the orientation averaging step. Comparing various modifications (different type of inclusion, ideal path of the fiber tow) suggests, perhaps even intuitively, almost negligible sensitivity of the solution

of the heat conduction problem to mutual interlacing of individual tows in comparison with the solution of the elasticity problem. This is mainly attributed to a relative flatness of the reinforcing yarns in individual plies of the laminate. In view of this, one may even offer the possibility of estimating the effective mesoscopic conductivities by simply assuming two systems of perpendicular fiber tows with no interlacing, thereby completely avoiding the orientation averaging step. But bear in mind that such a “drastic” simplification can hardly be generalized and is certainly not acceptable in the case of elasticity. To discriminate between various approaches is therefore difficult.

Comparison with experimental measurements is in principle twofold but also inconclusive. On the one hand it clearly supports the use of the proposed uncoupled multi-scale approach and the two-step homogenization scheme on individual scales to arrive at the predictions of the effective macroscopic thermal conductivities. Furthermore, at least quantitatively, the Mori-Tanaka method proved its applicability in the solution of complicated textile composites. These remarks have already been put forward in (Skoček *et al.*, 2008) with regard to the problem of effective elastic properties. To judge, on the other hand, the pertinence and reliability of the MT method solely by comparing the predicted and measured values, which may deny it, is certainly insufficient. While all deficiencies of the presented homogenization strategy were openly discussed, errors associated with experimental measurements were not mentioned and are not available.

In summary, focusing only on the quantitative perspective, the Mori-Tanaka method combined with popular multi-scale homogenization approach is viable and presents a suitable and efficient alternative to periodic homogenization typically based on finite element analysis.

## Acknowledgment

The authors would like to thank M. Kopáčková for assisting us with the solution of the transformation problem presented in Section 4.2. The financial support provided by the GAČR Grant No. 106/07/1244 and partially by the research project CEZ MSM 684077003 is also gratefully acknowledged.

## References

- Benveniste Y (1987). A new approach to the application of Mori-Tanaka theory in composite materials, *Mechanics of Materials* **6**, 147–157.
- Benveniste Y, Chen T and Dvorak G (1990). The effective thermal conductivity of composites reinforced by coated cylindrically orthotropic fibers, *Journal of Applied Physics* **67**(6), 2878–2884.

- Chen T and Yang S H (1995). The problem of thermal conduction for two ellipsoidal inhomogeneities in an anisotropic medium and its relevance to composite materials, *Acta Mechanica* **111**, 41–58.
- Dvorak G and Sejnoha M (1996). Initial failure maps for ceramic and metal matrix composites, *Modelling Simul. Mater. Sci. Eng.* **4**, 553–580.
- Eshelby J (1957). The determination of the elastic field of an ellipsoidal inclusion and related problems, *Proceeding of Royal Society, Series A* **241**, 376–396.
- Gommers B, Verpoest I and Van Houtte P (1998). The Mori-Tanaka method applied to textile composite materials, *Acta Materialia* **46**(6), 2223–2235.
- Hatta H and Taya M (1986). Equivalent inclusion method for steady state heat conduction in composites, *International Journal of Engineering Science* **24**, 1159–1170.
- Hellmich C and Ulm F J (2005). Drained and undrained poroelastic properties of healthy and pathological bone: a poro-micromechanical investigation, *Transp Porous Med* **58**, 243–268.
- Huysmans G, Verpoest I and Van Houtte P (1998). A poly-inclusion approach for the elastic modelling of knitted fabric composites, *Acta Materialia* **46**(9), 3003–3013.
- Jeong H, Hsu D and Liaw P (1998). Anisotropic Conductivities of Multiphase Particulate Metal-Matrix Composites, *Composite Science and Technology* **58**, 65–76.
- Košková B and Vopička S (2001). Determination of yarn waviness parameters for C/C woven composites, in *Proceedings of International Conference CARBON '01*, Lexington (KY,USA), pp. 1–6.
- Kubičár L, Boháč V and Vretenár V (2002). Transient methods for the measurement of thermophysical properties: The pulse transient method, *High Temperatures - High Pressures* **34**, 505–514.
- Kuhn J L and Charalambides P G (1999). Modeling of Plain Weave Fabric Composite Geometry, *Journal of Composite Materials* **33**(3), 188–220.
- Lackner R, Spiegl M, Blab R and Eberhardsteiner J (2005). Is Low-Temperature Creep of Asphalt Mastic Independent of Filler Shape and Mineralogy? - Arguments from Multiscale Analysis, *Journal of Materials in Civil Engineering, ASCE* **15**, 485–491.
- LIM (2008). *System Lucia G, User guide*, LUCIA – Laboratory Universal Computer Image Analysis, <http://www.laboratory-imaging.com>.
- Mori T and Tanaka K (1973). Average stress in matrix and average elastic energy of elastic materials with misfitting inclusions, *Acta Metallurgica* **21**, 571.
- Ohlhorst C W (1997). *Thermal Conductivity Database of Various Structural Carbon Carbon Composite Materials*, NASA Technical Memorandum 4787, Lanley Research Center, Hampton, Virginia.
- Piat R, Tsukrov I, Mladenov N, Guellali M, Ermel R, Beck E and Hoffman M (2007). Material modeling of the CVI-infiltrated carbon felt II. Statistical study of the microstructure, numerical analysis and experimental validation, *Composite Science and Technology* **66**(15), 2769–2775.
- Piat R, Tsukrov I, Mladenov N, Verijenko M, Guellali M, Schnack E and Hoffman M (2007). Material modeling of the CVI-infiltrated carbon felt I. Basic formulae, theory and numerical experiments, *Composite Science and Technology*

- 66(15), 2997–3003.
- Rektorys K, ed. (1994). *Survey of applicable mathematics: Volume II*, Vol. 281 of *Mathematics and its Applications*, second revised edn, Kluwer Academic Publishers Group, Dordrecht.
- Skoček J, Zeman J and Šejnoha M (2008). Effective properties of Carbon-Carbon textile composites: application of the Mori-Tanaka method, *Modelling and Simulation in Materials Science and Engineering* **0**, 0–0. Accepted.
- Šejnoha M, Valenta R and Zeman J (2004). Nonlinear Viscoelastic Analysis of Statistically Homogeneous Random Composites, *International Journal for Multiscale Computational Engineering* **2**(4), 645–673.
- Šejnoha M and Zeman J (2002). Overall viscoelastic response of random fibrous composites with statistically quasi uniform distribution of reinforcements, *Computer Methods in Applied Mechanics and Engineering* **191**(44), 5027–5044.
- Šejnoha M and Zeman J (2008). Micromechanical modeling of imperfect textile composites, *International Journal of Engineering Science* **46**, 513–526.
- Šmilauer V and Bittnar Z (2006). Microstructure-based micromechanical prediction of elastic properties in hydrating cement paste, *Cement and Concrete Research* **36**(9), 1708–1718.
- Tomková B (2004). Study of porous structure of C/C composites, in *International Conference ICAPM*, Evora, Portugal, pp. 379–387.
- Tomková B and Košková B (2004). The porosity of plain weave C/C composite as an input parameter for evaluation of material properties, in *International Conference Carbon 2004*, Providence, USA, p. 50.
- Tomková B, Šejnoha M, Novák J and Zeman J (2008). Evaluation of Effective Thermal Conductivities of Porous Textile Composites, *International Journal for Multiscale Computational Engineering* **6**(2), 153–168.
- TORAYCA (2008). *Technical data sheet, Toroyca T800H*, Toray Carbon Fibers America, <http://www.torayusa.com>.
- Tsukrov I, Piat R, Novak J and Schnack E (2005). Micromechanical Modeling of Porous Carbon/Carbon Composites, *Mechanics of Advanced Materials and Structures* **12**, 43–54.
- Vopička S (2004), Popis geometrie vyztužujícího systému v tkaninových kompozitech [Description of geometry of textile composites reinforcing system], PhD thesis, Technical University of Liberec. In Czech.
- Zeman J and Šejnoha M (2001). Numerical evaluation of effective properties of graphite fiber tow impregnated by polymer matrix, *Journal of the Mechanics and Physics of Solids* **49**(1), 69–90.
- Zeman J and Šejnoha M (2004). Homogenization of balanced plain weave composites with imperfect microstructure: Part I – Theoretical formulation, *International Journal for Solids and Structures* **41**(22–23), 6549–6571.